Collaborative Control of DFIG System During Network Unbalance Using Reduced-Order Generalized Integrators

Peng Cheng and Heng Nian, *Member, IEEE*

***Abstract*—The paper presents a collaborate control for the rotor-side converter (RSC) and grid-side converter (GSC) of a doubly fed induction generator (DFIG) generation system during network unbalance. In this study, the RSC is controlled to reduce the torque ripples, and three selectable control targets for the GSC, i.e., balanced total currents, and constant total active or reactive power into the grid from the overall system are identified to reduce the impacts of the negative-sequence voltage on the DFIG system performance. A reduced-order generalized integrator is employed, which is implemented in the positive synchronous reference frame. Based on the math model, the impacts of the limited dc voltage, as well as the rejection capability on negative-sequence voltage of the proposed control strategy, have been investigated. Finally, the simulation and experimental results are provided to demonstrate the effectiveness of the proposed collaborative control strategy.**

***Index Terms*—Collaborate control, doubly fed induction generator (DFIG), network unbalance, reduced-order generalized integrator (ROGI).**

I. Introduction

WIND POWER generation has attracted considerable attention due to the aggravating energy crisis and growing environment concerns. Among the different types of wind turbine generation systems, doubly fed induction generators (DFIGs) have been widely equipped due to the advantages including variable-speed constant-frequency operation, flexible power control and a smaller converter rating, compared with the fixed-speed induction generators or synchronous generators-based wind power system [1]–[3].

Since wind turbine generation systems have been being widely installed in the remote and offshore areas, the long transmission lines are required to transfer the power, which may cause the unstable voltage disturbances in the point of common coupling. Among all the disturbances, the voltage imbalances are more frequent and severe for the wind turbine. Thus, power system operators, such as E.ON of Germany [4], REE.MC of Spanish [5], Energinet.dk of Denmark [6], and State Grid Corporation of China [7], have given out the critical grid codes which require that the wind turbine generation systems are able to withstand a 2% steady-state and 4% short-time voltage imbalance without tripping [7].

Manuscript received February 16, 2014; revised June 29, 2014 and August 25, 2014; accepted October 13, 2014. Date of publication November 5, 2014; date of current version May 15, 2015. Paper no. TEC-00049-2014.

The authors are with the College of Electrical Engineering, Zhejiang University, Hangzhou 310027, China (e-mail: cheng_peng@zju.edu.cn; nianheng@zju.edu.cn).

Color versions of one or more of the figures in this paper are available online at http://ieeexplore.ieee.org.

Digital Object Identifier 10.1109/TEC.2014.2363671

In [8] and [9], the improved rotor current control schemes are designed for the rotor-side converter (RSC) under severe and short-time balanced fault conditions. Then, focused on the network voltages with low imbalance factor for a long time, several investigations have been proposed to improve the DFIG system performance [10]–[23]. The typical RSC control strategy employs two proportion integral (PI) current regulators implemented in the positive and negative synchronous reference frame, respectively [10]–[12]. However, the sequence decomposing process of both positive- and negative-sequence components in the control loop is inevitable, which would introduce the time delay and degrade the dynamic performance. The study in [13] and [14] proposed a current control scheme using proportional integral plus resonant (PI-R) regulators to implement the precise control of both positive and negative-sequence currents. In [10]–[14], the calculations of the rotor current references are based on the positive- and negative-sequence voltages. Besides, these calculations are highly dependent on the generator parameters. In [15] and [16], the compensating rotor voltage was calculated by either the calculated compensating rotor current values [15] or the generator torque ripples [16]. The compensation controllers must be particularly designed and the current controllers must be carefully tuned, which is a computational burden for digital signal processor (DSP) based implementation.

Similarly, the operation of gird-connected voltage-source converter (GC-VSC) on the unbalanced voltage have been studied in [17]–[19], in which the dual current controllers implemented in both the positive and negative synchronous reference frame [17], a PI-R implemented in the positive synchronous reference frame reference frame [18] and a proportional plus resonant (P-R) implemented in the stationary reference frame reference frame [19] are adopted.

However, these investigations are only focus on either DFIG or grid-side converter (GSC). In order to improve the operation capability and output power quality of DFIG system to satisfy the requirements, it is necessary to develop a collaborative control strategy for DFIG's RSC and GSC. In the previous studies [20]–[23], several coordinated control schemes based on a dual PI current controller [20] or a main controller implemented and an auxiliary controller [21], or a PI-R current controller [22], or a P-R current controller [23], have been proposed. From the view of the specific grid codes and the operation requirements, three alternative control targets for GSC, i.e., balanced and sinusoidal total currents, constant total active power or reactive power are identified in [23] to improve the grid connection

performance and output power quality. However, in these coordinated controls, the sequential decomposition of the voltages is still necessary, which may cause a negative impact on the dynamic responses. The control targets implementation is dependent on how accurately the command current values can be calculated, which requires the accurate DFIG system parameters.

The main objective of this paper is to develop a collaborative control strategy for both DFIG's RSC and GSC under the unbalanced grid voltage, which can achieve the different control targets for the overall DFIG system, i.e., balanced total currents, constant active power or reactive power. In this scheme, reduced-order generalized integrators (ROGIs) are employed to eliminate the calculations of the negative sequence current references and the decompositions of the positive- and negative-sequence voltages and currents. Thus, a simple implementation can be obtained and the dynamic responses of the DFIG system can behave faster and smoother. This paper will be organized as follows. Section II briefly describes DFIG typical performance during network unbalance. In Section III, a control scheme consisting of PI regulators and ROGIs tuned at twice grid frequency is designed, where three control targets are identified. Then, the impacts of the limited dc voltage and the rejection capability of the negative-sequence voltage are analyzed in Sections IV and V. Sections VI and VII present the simulation and experimental results, respectively. Finally, Section VIII draws the conclusions.

II. DFIG Behavior During Network Unbalance

For a DFIG system, the main objective of RSC is to regulate the stator output active and reactive powers while the GSC maintains the common dc-link voltage. Since the detailed model of both DFIG's RSC and GSC during network unbalance has been investigated in [10]–[11], [17], and [26], the useful descriptions for the demonstrations in the following sections are given here.

A. RSC (DFIG)

The DFIG model in this study is based on the stator voltage orientation (SVO). All the voltages and currents contain both positive- and negative-sequence components of the unbalanced voltage. Thus, these terms can be expressed on the basis of positive- and negative-sequence components in the positive $(dq)^+$ and negative $(dq)^-$ synchronous reference frame as

$$\boldsymbol{F}^+_{dq} = \boldsymbol{F}^+_{dq+} + \boldsymbol{F}^+_{dq-} = \boldsymbol{F}^+_{dq+} + \boldsymbol{F}^-_{dq-}e^{-j2\omega_1 t} \tag{1}$$

where vector $\boldsymbol{F}$ represents voltage $\boldsymbol{U}$, current $\boldsymbol{I}$, and flux $\boldsymbol{\psi}$, ω_1 is synchronous angular speed, superscripts $+$, $-$ represent $(dq)^+$ and $(dq)^-$ reference frame, subscripts $+$, $-$ represent the positive- and negative-sequence components, subscripts d, q represent components at the d-q axis, subscripts s, r represent the stator and rotor, respectively.

Fig. 1 shows the DFIG equivalent circuit in the $(dq)^+$ reference frame. Then, the stator/rotor voltage and flux can be given by

$$\boldsymbol{U}^+_{sdq} = R_s\boldsymbol{I}^+_{sdq} + d\boldsymbol{\psi}^+_{sdq}/dt + j\omega_1\boldsymbol{\psi}^+_{sdq} \tag{2a}$$

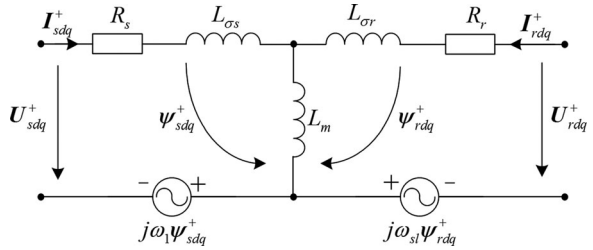

Fig. 1. DFIG equivalent circuit on the $(dq)^+$ reference frame.

$$\boldsymbol{U}^+_{rdq} = R_r\boldsymbol{I}^+_{rdq} + d\boldsymbol{\psi}^+_{rdq}/dt + j\omega_{sl}\boldsymbol{\psi}^+_{rdq} \tag{2b}$$

$$\boldsymbol{\psi}^+_{sdq} = L_s\boldsymbol{I}^+_{sdq} + L_m\boldsymbol{I}^+_{rdq} \tag{3a}$$

$$\boldsymbol{\psi}^+_{rdq} = L_m\boldsymbol{I}^+_{sdq} + L_r\boldsymbol{I}^+_{rdq} \tag{3b}$$

where R_s and R_r are stator and rotor resistances, ω_r is rotor angular speed, and $\omega_{sl} = \omega_1 - \omega_r$ is slip angular speed, $L_s = L_m + L_{\delta s}$ and $L_r = L_m + L_{\delta r}$ are the self-inductance of stator and rotor windings, $L_{\delta s}$, $L_{\delta r}$ and L_m are stator and rotor leakage inductances and mutual inductance, respectively.

According to (2a), (2b), (3a) and (3b), the rotor voltage in the $(dq)^+$ frame can be represented as

$$\boldsymbol{U}^+_{rdq} = \sigma L_r\, d\boldsymbol{I}^+_{rdq}/dt + \boldsymbol{E}_{rdq} \tag{4}$$

where $\sigma = 1 - L_m^2/(L_sL_r)$ is the leakage factor and $\boldsymbol{E}_{rdq}$ is the equivalent rotor back electromagnetic force and given as

$$\begin{aligned}\boldsymbol{E}_{rdq} = {} & (R_r + \boldsymbol{j}\sigma L_r\omega_{sl})\boldsymbol{I}^+_{rdq} \\ & + L_m(\boldsymbol{U}^+_{sdq} - R_s\boldsymbol{I}^+_{sdq} - j\omega_r\boldsymbol{\psi}^+_{sdq})/L_s\end{aligned} \tag{5}$$

According to (1), assuming that the stator resistance is ignored [13], [26], (2a) can be written as

$$\begin{aligned}\boldsymbol{U}^+_{sdq} \approx {} & d(\boldsymbol{\psi}^+_{sdq+} + \boldsymbol{\psi}^-_{sdq-}e^{-j2\omega_1 t})/dt \\ & + j\omega_1(\boldsymbol{\psi}^+_{sdq+} + \boldsymbol{\psi}^-_{sdq-}e^{-j2\omega_1 t}) \\ = {} & j\omega_1\boldsymbol{\psi}^+_{sdq+} - j\omega_1\boldsymbol{\psi}^-_{sdq-}e^{-j2\omega_1 t}.\end{aligned} \tag{6}$$

Under the unbalanced supply, the stator current contains both positive- and negative-sequence components. According to (1) and (6), the stator current can be expressed as

$$\boldsymbol{I}^+_{sdq} = (I^+_{sd+} + jI^+_{sq+}) + (I^-_{sd-} + jI^-_{sq-})e^{-j2\omega_1 t} \tag{7}$$

where

$$\begin{bmatrix} I^+_{sd+} \\ I^+_{sq+} \\ I^-_{sd-} \\ I^-_{sq-} \end{bmatrix} = \frac{1}{\omega_1 L_s}\begin{bmatrix} U^+_{sq+} \\ -U^+_{sd+} \\ -U^-_{sq-} \\ U^-_{sd-} \end{bmatrix} - \frac{L_m}{L_s}\begin{bmatrix} I^+_{rd+} \\ I^+_{rq+} \\ I^-_{rd-} \\ I^-_{rq-} \end{bmatrix}. \tag{8}$$

Consequently, by neglecting the stator copper loss, the stator active and reactive powers outputted can be calculated as [10], [13],

$$\begin{aligned}P_s = {} & P_{s0} + P_{s2} = P_{s0} + P_{ss2}\sin(2\omega_1 t) + P_{sc2}\cos(2\omega_1 t) \\ Q_s = {} & Q_{s0} + Q_{s2} = Q_{s0} + Q_{ss2}\sin(2\omega_1 t) + Q_{sc2}\cos(2\omega_1 t).\end{aligned} \tag{9}$$

Similarly, based on (6), the electromagnetic torque is given as [10], [13]

$$\begin{aligned} T_e &= -1.5n_p\mathrm{Re}\left[j\boldsymbol{\psi}^+_{sdq}\times\hat{\boldsymbol{I}}^+_{rdq}\right]L_m/L_s \\ &= -1.5n_p\mathrm{Re}\left[\boldsymbol{U}^+_{sdq}\times\hat{\boldsymbol{I}}^+_{rdq}\right]L_m/L_s \\ &= T_{e0}+T_{e2}=T_{e0}+T_{es2}\sin(2\omega_1 t)+T_{ec2}\cos(2\omega_1 t) \end{aligned} \tag{10}$$

where

$$\begin{bmatrix} T_{e0} \\ T_{es2} \\ T_{ec2} \end{bmatrix} = 1.5\frac{n_pL_m}{\omega_1 L_s}\begin{bmatrix} -U^+_{sd+} & -U^+_{sq+} & U^-_{sd-} & U^-_{sq-} \\ U^-_{sq-} & -U^-_{sd-} & U^+_{sq+} & -U^+_{sd+} \\ U^-_{sd-} & U^-_{sq-} & -U^+_{sd+} & -U^+_{sq+} \end{bmatrix}\begin{bmatrix} I^+_{rd+} \\ I^+_{rq+} \\ I^-_{rd-} \\ I^-_{rq-} \end{bmatrix}. \tag{11}$$

B. GSC

The GSC behaves as a GC-VSC under unbalanced supply. The voltages and currents consist of both positive- and negative-sequence components. Thus, the GSC under unbalanced supply can be represented in the $(dq)^+$ frame as

$$\boldsymbol{U}^+_{gdq} = -L_g\frac{d\boldsymbol{I}^+_{gdq}}{dt}+\boldsymbol{E}_{gdq} \tag{12}$$

where U^+_{gdq} refers to the control voltage produced by the GSC

$$\boldsymbol{E}_{gdq} = \boldsymbol{U}^+_{sdq} - R_g\boldsymbol{I}^+_{gdq} - j\omega_1 L_g\boldsymbol{I}^+_{gdq}. \tag{13}$$

In [13] and [17], the active and reactive power from the GSC to the network can be expressed as

$$\begin{aligned} P_g &= P_{g0}+P_{g2}=P_{g0}+P_{gs2}\sin(2\omega_1 t)+P_{gc2}\cos(2\omega_1 t) \\ Q_g &= Q_{g0}+Q_{g2}=Q_{g0}+Q_{gs2}\sin(2\omega_1 t)+Q_{gc2}\cos(2\omega_1 t). \end{aligned} \tag{14}$$

Accordingly, the total current and powers into the network from the overall DFIG system can be represented as

$$\boldsymbol{I}^+_{tdq} = \boldsymbol{I}^+_{sdq}+\boldsymbol{I}^+_{gdq} \tag{15}$$

$$S_t = P_t+\boldsymbol{j}Q_t = -1.5\boldsymbol{U}^+_{sdq}\times\hat{\boldsymbol{I}}^+_{tdq} \tag{16}$$

where subscript *t* represents the overall system.

According to (9), (14), and (16), the power of DFIG system into the grid can be calculated and expressed as

$$\begin{bmatrix} P_{X0} \\ Q_{X0} \\ P_{Xs2} \\ P_{Xc2} \\ Q_{Xs2} \\ Q_{Xc2} \end{bmatrix} = -1.5\begin{bmatrix} U^+_{sd+} & U^+_{sq+} & U^-_{sd-} & U^-_{sq-} \\ U^+_{sq+} & -U^+_{sd+} & U^-_{sq-} & -U^-_{sd-} \\ U^-_{sq-} & -U^-_{sd-} & -U^+_{sq+} & U^+_{sd+} \\ U^-_{sd-} & U^-_{sq-} & U^+_{sd+} & U^+_{sq+} \\ -U^-_{sd-} & -U^-_{sq-} & U^+_{sd+} & U^+_{sq+} \\ U^-_{sq-} & -U^-_{sd-} & U^+_{sq+} & -U^+_{sd+} \end{bmatrix}\cdot\begin{bmatrix} I^+_{Xd+} \\ I^+_{Xq+} \\ I^-_{Xd-} \\ I^-_{Xq-} \end{bmatrix} \tag{17}$$

where subscript $X = s, g, t$ represents the stator power, the GSC power, and the total power into the grid, respectively.

Since the *d*-axis in the $(dq)^+$ reference frame is aligned with the positive sequence stator voltage, (11) and (17) can be simplified by taking into account $U^+_{sq+}=0$ in the SVO model.

III. Collaborative Control of Both RSC and GSC

A. Control Design

In order to enhance the uninterrupted operation capability of DFIG system, a collaborative control scheme is adopted for DFIG's RSC and GSC. This collaborate control can provide the overall DFIG system with enhanced performance and high output power quality to meet the system requirements, including balanced total current, constant total active or reactive power. This control scheme is implemented in the positive $(dq)^+$ synchronous reference frame. The positive- and negative-sequence fundamental components are converted into the dc signals and twice-order harmonic signals of $2\omega_1$, respectively. As indicated in [24], PI controllers can only regulate the dc components of the feedbacks (positive-sequence fundamental components) to track the dc references due to the lower amplitude responses at high frequencies. Thus, the average active and reactive powers can be still regulated by PI controllers. A generalized integrator tuned at the twice grid frequency can be selected to suppress the $2\omega_1$ components. Although both ROGI and second-order generalized integrator (SOGI) can provide the infinite gain with the certain sinusoidal signal, ROGI can provide a discrimination capability between the positive- and negative-sequence signals, which is an attractive feature, as shown in the followings.

Fig. 2 shows the collaborative control scheme for DFIG's RSC and GSC under unbalanced voltage conditions. The proposed scheme consists of two regulators in either RSC or GSC: 1) PI current controller; and 2) ROGI tuned at twice grid frequency, providing infinite gain only to $-2\omega_1$ ac signals. The PI controllers and $2\omega_1$ ROGIs transfer functions are given as

$$G_{\mathrm{PI}}(s) = k_p + k_i/s \tag{18}$$

$$G_R(s) = k_r\omega_c/\left(s+j2\omega_1+\omega_c\right) \tag{19}$$

where k_p, k_i, and k_r are the proportion, integral and resonant gain in the continuous-time system, respectively, ω_c is a cut-off frequency for determining the width of the frequency $2\omega_1$, which is generally set around 5–15 rad/s, similar to SOGIs [23].

In RSC, since the generator torque ripples may deteriorate the lifetime of the drive shaft and mechanical units, it is necessary to eliminate the twice frequency torque ripples when DFIG works on the unbalanced voltage. Different from the solutions in [20]–[23] to control the negative-sequence rotor currents tracking the commanded values, it is noted that the torque is directly regulated by a ROGI tuned at $-2\omega_1$ in the proposed control strategy. The negative-sequence rotor voltage reference is generated directly by controlling the torque instead of controlling the rotor currents; thus, the calculations of the negative-sequence current references based on the positive- and negative-sequence voltages can be eliminated. Thus, based on (10), the feedback

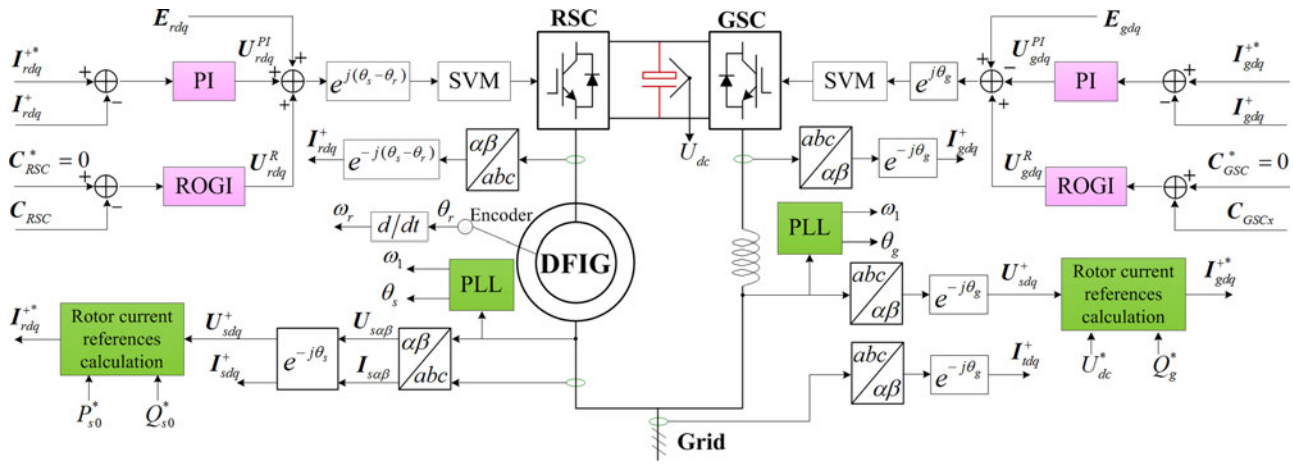

Fig. 2. Schematic diagram of the proposed collaborative control strategy for DFIG's RSC and GSC.

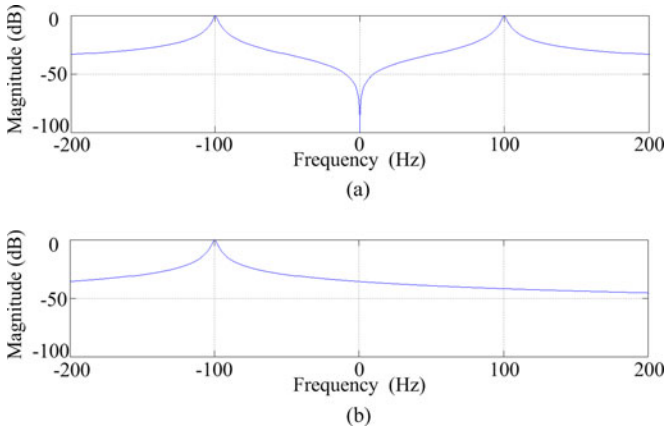

Fig. 3. Bode diagram of SOGI and ROGI: $k_r = k_s = 1$, $\omega_c = 10$ rad/s. (a) Magnitude responses of SOGI. (b) Magnitude responses of ROGI.

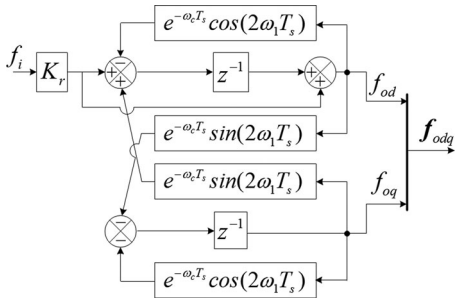

Fig. 4. Discrete-time implementation of a ROGI with a single pole.

references of this ROGI can be given as

$$C_{\mathrm{RSC}} = -T_e = 1.5 n_p L_m (U_{sd}^{+} I_{rd}^{+} + U_{sq}^{+} I_{rq}^{+})/(\omega_1 L_m). \quad (20)$$

This ROGI can only provide the high gain for the selected $-2\omega_1$ ac signals, while the ac signals of other frequencies and the dc signals can be blocked. In other words, the ROGI only regulates the $2\omega_1$ components of the torque and has no control capability of other frequency components. Thus, the torque can be used to replace the twice frequency ripples as the feedback references of the ROGI. Since the ROGI can almost achieve zero steady-state errors at $2\omega_1$, the twice frequency ripples can be eliminated if the commanded reference of the ROGI in the RSC can be set as zero, i.e., $C_{\mathrm{RSC}}^{*} = 0$.

During the balanced grid conditions, the torque is constant without 100 Hz ripples and the ROGI's output is zero. Thus, ROGIs have no impacts on the rotor current control loop of the active and reactive power regulation. However, during network unbalance, since the torque contains 100 Hz ripple, as analyzed previously, the ROGI's output is a vector rotating in the negative direction. The *d*- and *q*-axes components of this vector are added to the *d*- and *q*-axes rotor voltage references produced by PI controllers in the rotor current control loop. Then, the required rotor voltages are generated, which can be used to control the DFIG.

As for the GSC, PI controllers in the current control loop are used to maintain a common dc-link voltage regardless of the magnitude and direction of rotor power flow. In the view of the grid requirements, the GSC can be controlled to achieve one of the following targets [23].

Target I: To ensure balanced total currents from the overall system into the network, i.e., $I_{gd-}^{-} = I_{gq-}^{-} = 0$.

Target II: To ensure no double-frequency oscillations in the total active power, i.e., $P_{ts2} = P_{tc2} = 0$.

Target III: To ensure no double-frequency oscillations in the total reactive power, i.e., $Q_{ts2} = Q_{ts2} = 0$.

For these control targets, by using the proposed control strategy in Fig. 2, different feedback references can be designed as follows.

For *Target I*, to ensure no negative-sequence currents into the grid, the feedback of ROGI can be expressed as

$$C_{\mathrm{GSC1}} = -I_{td-}^{-} - jI_{tq-}^{-}. \quad (21)$$

For *Target II*, to remove the oscillations in the total active power, based on (17), the feedback can be obtained as

$$C_{\mathrm{GSC2}} = -P_t = 1.5(U_{sd}^{+} I_{td}^{+} + U_{sq}^{+} I_{tq}^{+}). \quad (22)$$

TABLE I
PARAMETERS OF THE TESTED DFIG

Rated power	2.0 MW	Rated voltage	690 V
R_s	0.0083 p.u.	DC voltage	1150 V
R_r	0.0069 p.u.	L_{δ_s}	0.090 p.u.
L_m	4.810 p.u.	L_{δ_r}	0.065 p.u.
Stator/rotor turns ratio	0.33	Pole number	0.33

While for *Target III*, to remove the oscillations in the total reactive power, based on (17), the feedback can be calculated as

$$C_{\mathrm{GSC3}} = jQ_t = j1.5(U_{sd}^{+}I_{tq}^{+} - U_{sq}^{+}I_{td}^{+}). \tag{23}$$

Similar to the RSC, ROGIs are employed in the GSC control system. Since the ROGI can provide adequate gain only at $2\omega_1$ and attenuate other frequency components, the electromagnetic quantities, including the current, the total active and reactive power, instead of the respective pulsations can be directly controlled by the ROGI in this scheme. The twice frequency pulsations can be eliminated if the commanded value of the ROGI in the GSC can be set as zero, i.e., $C_{\mathrm{GSC}}^{*} = 0$. During network unbalance, similar to the RSC, the *d*- and *q*-axes components of the ROGI's output are added to the *d*- and *q*-axes voltage references produced by PI controllers in the current control loop, respectively. Then, the commanded voltage of the GSC is produced to control the GSC.

Compared to the existing control strategies, including the PI + R method [13] and P + R method [23], the proposed control strategy has the advantages: 1) simple implementations due to the elimination of the calculations of the negative-sequence current reference; and 2) fast dynamic responses due to the avoidance of the sequential decompositions of the positive- and negative-sequence components.

B. ROGI

Since the negative-sequence components appears at $-2\omega_1$ in the $(dq)^{+}$ reference frame, the ROGIs are selected to control the $-2\omega_1$ components due to the frequency discrimination capability between $2\omega_1$ and $-2\omega_1$ [25]. In order to describe the advantages of ROGIs, the transfer function of the SOGI and ROGI will be given and compared in the proposed control scheme. Then, as shown in [13] and [23], SOGI can be described as

$$G_S(s) = k_s \cdot 2\omega_c s/(s^2 + 2\omega_c s + (2\omega_1)^2) \tag{24}$$

where k_s is the resonant gain, and ω_c is a cut-off frequency.

Based on (19) and (24), Fig. 3 shows the magnitude response of the SOGI and ROGI, in which the negative sign refers to the negative rotating direction. It can be seen that the ROGI only provides infinite gain to the $2\omega_1$ ac sinusoidal signal rotating in the negative direction, while SOGI provides infinite gain with both $2\omega_1$ and $-2\omega_1$ ac signals. Thus, ROGI's output is a vector of $2\omega_1$ rotating in the negative direction, while SOGI's output is a sinusoidal scalar. Based on Eular's formula, this scalar can be divided into two components of $2\omega_1$ and $-2\omega_1$ vectors rotating in the opposite direction.

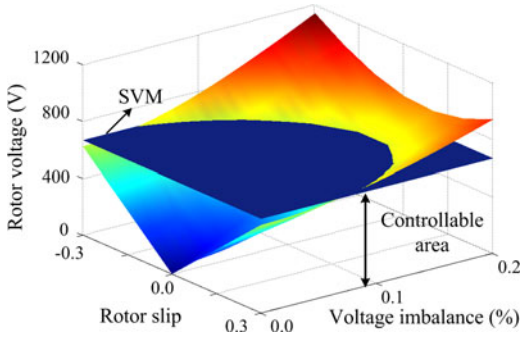

Fig. 5. Variations of rotor voltage with different rotor speeds and network voltage imbalances.

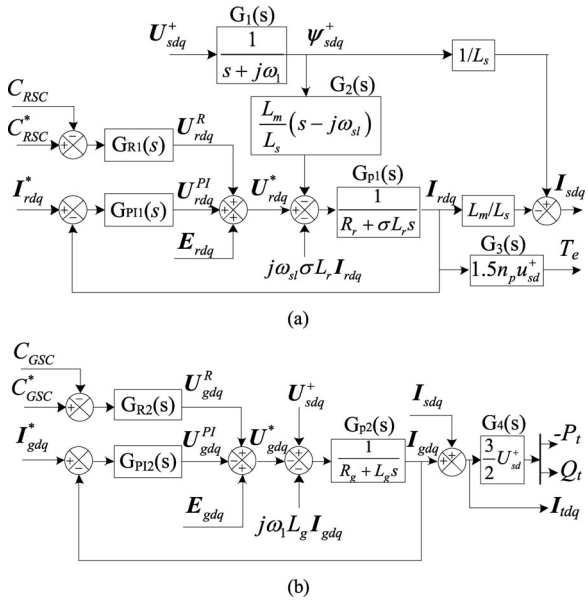

Fig. 6. Overall block diagram of the proposed control strategy: (a) RSC; and (b) GSC.

To make a clear comparison of SOGI and ROGI, taking the control scheme of RSC as an instance, the distinctions with ROGI and SOGI employed are discussed. In the RSC, based on (11), the torque is directly used as the feedback of the resonant controller, i.e., either ROGI or SOGI.

Assume that the torque during network unbalance can be expressed as $T_e = n + m \cdot \cos(2\omega_1 t + \varphi_0)$, where *n* and *m* represent the average value and the twice frequency amplitude, respectively. If a SOGI is adopted, the output of the resonant controller contains not only a positive-sequence component of $2\omega_1$ but also a negative-sequence component of $-2\omega_1$ in the $(dq)^{+}$ reference frame. Then, it can be calculated as

$$\begin{aligned} \boldsymbol{U}_{rdq}^{R} &= U_R \cdot \cos(2\omega_1 t + \varphi_0) \\ &= 0.5U_R e^{j(2\omega_1 t + \varphi_0)} + 0.5U_R e^{-j(2\omega_1 t + \varphi_0)} \end{aligned} \tag{25}$$

where U_R represents the amplitude of the SOGI output

Taking coordinate transformations from the $(dq)^{+}$ to $(\alpha\beta)$ reference frame, (25) can be written as

$$\boldsymbol{U}_{r\alpha\beta}^{R} = 0.5U_R e^{j\varphi_0} \cdot e^{j3\omega_1 t} + 0.5U_R e^{j\varphi_0} \cdot e^{-j\omega_1 t} \tag{26}$$

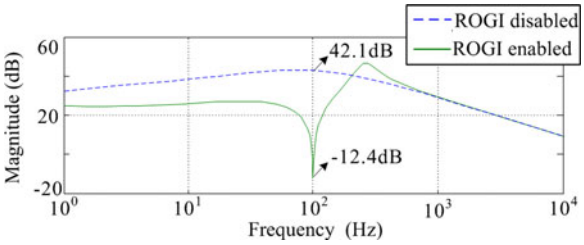

Fig. 7. Magnitude response of $F_T(s)$ ($k_{p1}=5, k_{i1}=30, k_{r1}=10$).

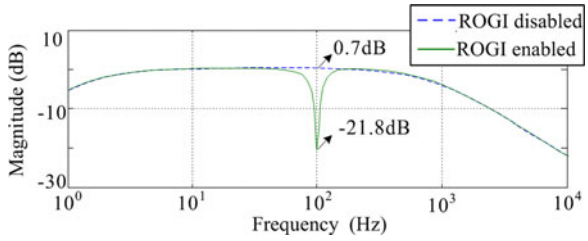

Fig. 8. Magnitude response of $F_{It}(s)$ ($k_{p2}=2, k_{i2}=15, k_{r2}=10$).

It is noted that the former is converted into a third-order harmonic voltage in the $(\alpha\beta)$ reference frame, which would produce third-order harmonic currents, while the latter is converted into a negative-sequence fundamental voltage and would not produce harmonic currents.

When a ROGI is adopted, the output only contains a negative-sequence component of $-2\omega_1$ in the $(dq)^+$ reference frame and can be obtained as

$$\boldsymbol{U}_{rdq}^{R} = 0.5U_R e^{-j(2\omega_1 t+\varphi_0)}. \tag{27}$$

It is pointing out that the third-order harmonic voltage is not produced under such conditions. Thus, ROGI can implement not only the $2\omega_1$ ac signal regulation but also third-order harmonic current elimination, which is particularly suitable for the grid-connected power conversion control with high-quality injected currents.

Since (19) has the complex j multiplier on the behalf of a cross-coupling term, its output in the $(dq)^+$ reference frame consists of d- and q-axes components. Its implementation in the discrete time must be presented for a DSP-based approach. Thus, based on $z=e^{sT_s}$, the discrete-time description of a ROGI with a pole in $-\omega_c - j2\omega_1$ can be described as

$$G_R(z) = \frac{Y(n)}{X(n)} = \frac{K_r(z+1)}{z - e^{-\omega_c T_s} e^{-j2\omega_1 T_s}} \tag{28}$$

where K_r is the resonant gain in the discrete-time system.

Fig. 4 shows the discrete-time implementation of (28), in which f_i and f_{odq} are the ROGI's input and output, and f_{od} and f_{oq} are the ROGI's outputs on the d- and *q-axes*, respectively. It can be seen that the ROGI output is a vector containing both d- and q-axes components. Furthermore, the output f_{odq} only rotates in the negative direction. Thus, (28) can be used to implement ROGIs in the discrete time for the proposed control scheme.

C. System Implementation

In Fig. 2, it can be seen that the collaborative control scheme for DFIG's RSC and GSC is mainly made up of two parts: phase-locked loop (PLL) and commanded voltage modulation. An improved PLL with a SOGI tuned at double the grid frequency, named R-PLL in [26], is employed to track the phase angle of the positive-sequence voltage for the coordinate transformations.

According to Fig. 2, the commanded rotor voltage consists of three parts: the PI output, the ROGI output, and the equivalent rotor back electromagnetic force. Then, the commanded rotor voltage for the RSC can be given as

$$\begin{aligned}\boldsymbol{U}_{rdq}^{+*} &= \boldsymbol{U}_{rdq}^{\mathrm{PI}} + \boldsymbol{U}_{rdq}^{R} + \boldsymbol{E}_{rdq} \\ &= G_{\mathrm{PI1}}(s)(\boldsymbol{I}_{rdq}^{+*} - \boldsymbol{I}_{rdq}^{+}) \\ &\quad + G_{R1}(s)(C_{\mathrm{RSC}}^{*} - C_{\mathrm{RSC}}) + \boldsymbol{E}_{rdq}\end{aligned} \tag{29}$$

where $\boldsymbol{U}_{rdq}^{\mathrm{PI}}$ is the PI output, $\boldsymbol{U}_{rdq}^{R}$ is the ROGI output, and C_{RSC} represents the feedbacks for the RSC according to (20).

Then, the commanded rotor voltage is transferred to the rotor stationary reference frame according to the voltage phase angle θ_s acquired by the R-PLL and the rotor angle θ_r acquired by the encoder, which can be written as

$$\boldsymbol{U}_{r\alpha\beta}^{*} = \boldsymbol{U}_{rdq}^{+*} e^{j(\theta_s - \theta_r)}. \tag{30}$$

In a similar way, the commanded voltage for the GSC can be represented as

$$\begin{aligned}\boldsymbol{U}_{gdq}^{+*} &= -\boldsymbol{U}_{gdq}^{\mathrm{PI}} + \boldsymbol{U}_{gdq}^{R} + \boldsymbol{E}_{gdq} \\ &= -G_{\mathrm{PI2}}(s)(\boldsymbol{I}_{gdq}^{+*} - \boldsymbol{I}_{gdq}^{+}) \\ &\quad + G_{R2}(s)(C_{\mathrm{GSC}}^{*} - C_{\mathrm{GSC}x}) + \boldsymbol{E}_{gdq}\end{aligned} \tag{31}$$

where $\boldsymbol{U}_{gdq}^{\mathrm{PI}}$ is the PI output, $\boldsymbol{U}_{gdq}^{R}$ is the ROGI output, $C_{\mathrm{GSC}x}(x=1,2,3)$ represents the different feedbacks for GSC according to the control targets, i.e., (21), (22), and (23).

Then, the voltage reference for the GSC is transformed from the $(dq)^+$ synchronous reference frame to the stationary reference frame using the phase angle θ_g obtained by R-PLL, and it can be expressed as

$$\boldsymbol{U}_{g\alpha\beta}^{*} = \boldsymbol{U}_{gdq}^{+*} e^{j\theta_g}. \tag{32}$$

Finally, with the commanded voltages shown in (30) and (32), a space vector modulation (SVM) is used to generate the required switching signal to control the RSC and GSC.

IV. Impacts of the Limited DC Voltage

Due to the limited dc voltage, the SVM cannot provide the adequate voltages for the DFIG control requirement during larger network unbalance. As indicated in [27], since the GSC is directly connected to the grid, there is no limited voltage issues for the GSC. Thus, this section will fully discuss the impacts of the limited dc voltage on the RSC.

According to (29), it is indicated that the commanded rotor voltage for the RSC consists of both the positive- and negative-sequence components based on the proposed method. Assuming that the initial phases of the positive- and negative-sequence

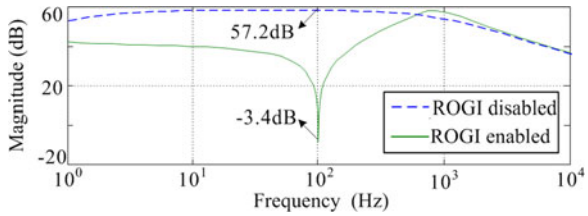

Fig. 9. Magnitude response of $F_{\mathrm{PQ}}(s)$ $(k_{p2} = 2, k_{i2} = 15, k_{r2} = 10)$.

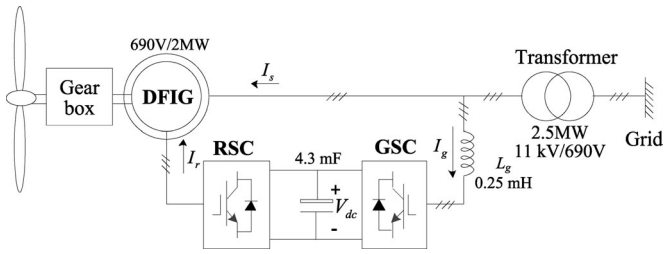

Fig. 10. Scheme of the simulation system.

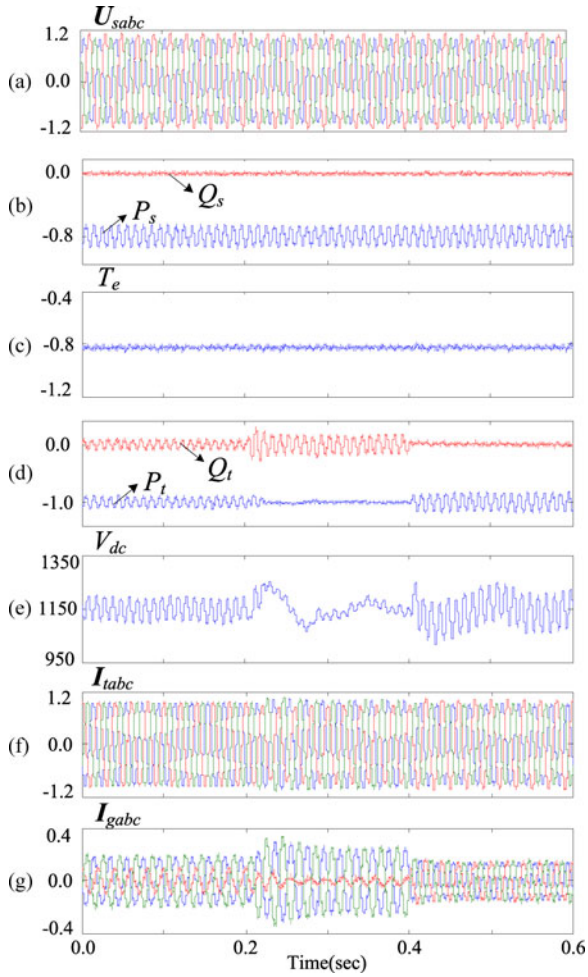

Fig. 11. Simulation results with different control targets: *Target I*, 0.0–0.2 s; *Target II*, 0.2–0.4 s; *Target III*, 0.4–0.6 s [(a) three-phase stator voltage (p.u.), (b) stator active and reactive powers (p.u.), (c) electromagnetic torque (p.u.), (d) total active and reactive powers (p.u.), (e) dc-link voltage (*V*), (e) three-phase total current (p.u.), and (g) three-phase grid current (p.u.)].

TABLE II
COMPARISONS AMONG THE ALTERNATIVE CONTROL TARGETS DURING NETWORK UNBALANCE

Control targets	Target I	Target II	Target III
I_t unbalance (%)	**0.7**	7.1	7.6
P_t pulsation (%)	±9.3	±**0.5**	±15.2
Q_t pulsation (%)	±7.5	±16.2	±**1.1**
V_{dc} pulsation (%)	±5.7	±1.3	±8.1

stator voltage are the same, the commanded rotor voltage under unbalanced supply can be represented as

$$U_{rm} = \sqrt{U_{rm+}^2 + U_{rm-}^2} \tag{33}$$

where U_{rm}, U_{rm+}, and U_{rm-} represent the amplitude of the rotor voltage, the positive-sequence component of rotor voltage, and the negative-sequence component of rotor voltage, respectively

$$U_{rm+} = \frac{L_m}{L_s}\left|1 - \frac{\omega_r}{\omega_1}\right| \cdot \frac{U_{sm+}}{N_{sr}} \tag{34a}$$

$$U_{rm-} = \frac{L_m}{L_s}\left|1 + \frac{\omega_r}{\omega_1}\right| \cdot \frac{U_{sm-}}{N_{sr}} \tag{34b}$$

where U_{sm+} and U_{sm-} are the amplitudes of the positive- and negative-sequence stator voltage, respectively.

Actually, N_{sr} is the stator/rotor turns radio and is usually set as 1/3–1/2 to reduce the current ratings of the RSC. As seen from (34a) and (34b), the required amplitude of the rotor voltage is determined not only by the rotor speed, but also by the negative-sequence value U_{sm-}. Besides, the amplitude of the rotor voltage is affected by the fixed turns radio N_{sr} of DFIG. In order to analyze the influence of dc voltage on DFIG control, a 2 MW DFIG is selected with the parameter as listed in Table I.

Fig. 5 shows the variations of rotor voltages with different rotor speeds and network voltage imbalances. When dc-bus voltage is fixed at 1150 V, the maximum output phase voltage amplitude using the SVM technique is 664 V. From the results in Fig. 5, it can be seen the following.

1) During balanced voltage conditions, the SVM can provide the adequate rotor voltage for DFIG control within the ±0.3 rotor slip.
2) Under unbalanced grid voltage conditions, higher voltage amplitudes are required, whose amplitude is approximately proportional to the rotor slip and the negative-sequence stator voltage.
3) Under the same voltage unbalance, the higher rotor speed requires the higher rotor voltage. Under a large voltage imbalance, the required rotor voltage may exceed the maximum voltage provided by the SVM, and thereby the generator would enter into the uncontrollable area above the SVM plane. Thus, the control targets of DFIG system cannot be fully achieved.

Thus, the main concerns should be focused on the limited rotor voltage under unbalanced grid voltage conditions. Only

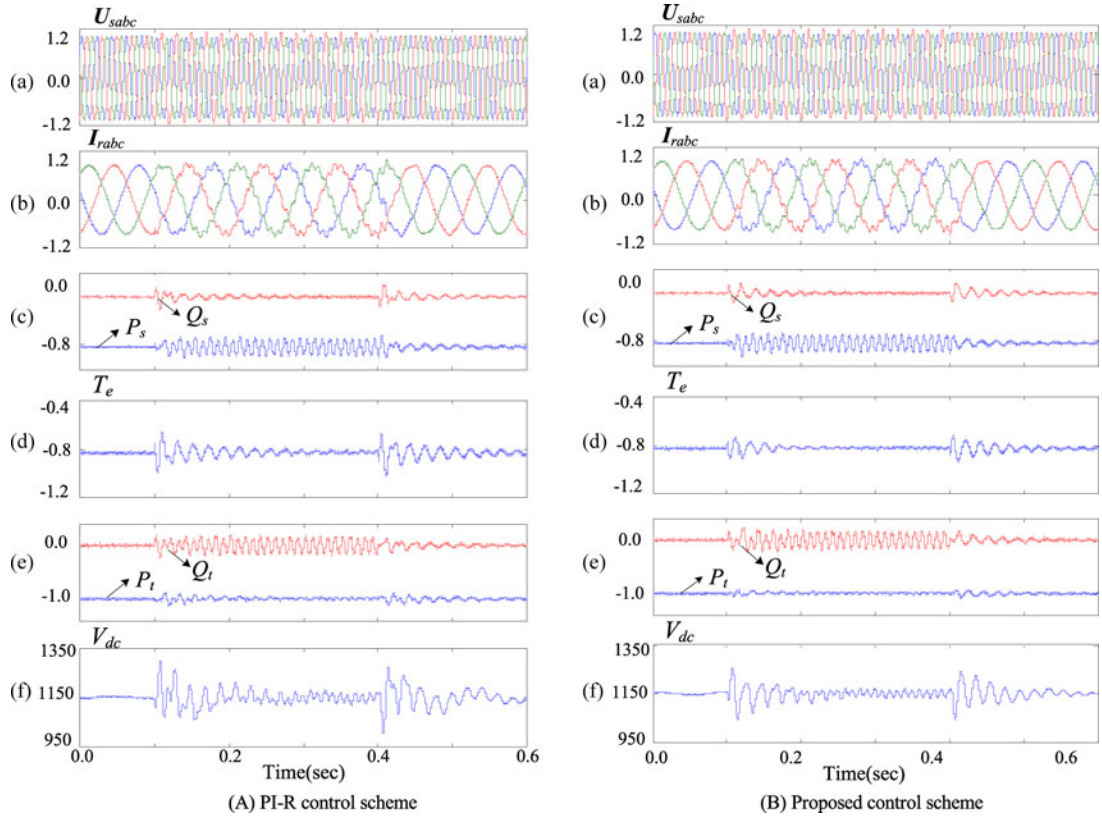

Fig. 12. Simulation results during a transient voltage unbalance of 10% [(a) three-phase stator voltage (p.u.), (b) three-phase rotor current (p.u.), (c) stator active and reactive powers (p.u.), (d) electromagnetic torque (p.u.), (e) total active and reactive powers (p.u.), and (f) dc-link voltage (*V*)].

when the RSC is capable of providing adequate rotor voltage, the proposed control targets can be fully achieved.

V. Control Performance Analysis

In order to implement the alternative control targets, the proposed collaborative control strategy should have the excellent rejection capability on the negative-sequence voltage disturbances. Thus, in order to verify the operation capability of the proposed control strategy, the rejection capability on negative-sequence voltage disturbances should be fully investigated.

Therefore, based on (4), (6), (8), (10), (12), (15), (17), and Fig. 2, the block diagram of both DFIG's RSC and GSC is shown in Fig. 6, where $G_{p1}(s) = 1/(R_r + \sigma L_r s)$, $G_{p2}(s) = 1/(R_g + L_g s)$, $G_1(s) = 1/(s + j\omega_1)$, $G_2(s) = (s + j\omega_{sl})L_m/L_s$, $G_3(s) = 1.5n_p U_{sd}^+$, and $G_4(s) = 1.5U_{sd}^+$. The DFIG parameters are shown in Table I.

Fig. 6 presents the control block of the collaborative control of both the RSC and GSC. Since the stator voltage is aligned with the *d*-axis, the *q*-axis voltage is approximately zero, which can be neglected to simplify the analysis. Besides, to investigate the impacts caused by the negative-sequence voltage, the positive-sequence fundamental voltage can be removed [28]. Thus, according to Fig. 6(a), in the proposed control scheme for the RSC, the transfer function from the negative-sequence voltage to the DFIG torque can be obtained as follows:

$$F_T(s) = \frac{T_e}{U_{sd-}^+} = \frac{-G_1(s)G_2(s)G_3(s)G_{p1}(s)}{1 + G_{\mathrm{PI1}}(s)G_{p1}(s) + G_{R1}(s)G_3(s)G_{p1}(s)}. \tag{37}$$

Fig. 7 shows the magnitude response of $F_T(s)$ based on the generator parameters in Table I, which represents the rejection capability of the negative-sequence voltage on the generator torque with the ROGI enabled and disabled. When the ROGI is enabled, the magnitude response at $2\omega_1$ decreases from 42.1 to -12.4 dB, which means that the proposed ROGI-based control strategy has enough suppression capability on the torque ripples caused by the negative-sequence stator voltage.

As for GSC, the different control targets can be obtained on the basis of the total currents, the sum of the grid currents and the stator currents. Thus, the transfer function of the negative-sequence voltage to the stator currents can be calculated as (38), shown at the bottom of the page.

$$F_{Is}(s) = \frac{I_{sd}}{U_{sd-}^+} = \frac{I_{sq}}{U_{sd-}^+} = \frac{G_1(s)G_2(s)G_{p1}(s)L_m/L_s}{1 + G_{\mathrm{PI1}}(s)G_{p1}(s) + G_{R1}(s)G_3(s)G_{p1}(s)} + \frac{G_1(s)/L_s + G_1(s)G_{\mathrm{PI1}}(s)G_{p1}(s)/L_s + G_1(s)G_{R1}(s)G_3(s)G_{p1}(s)/L_s}{1 + G_{\mathrm{PI1}}(s)G_{p1}(s) + G_{R1}(s)G_3(s)G_{p1}(s)}. \tag{38}$$

TABLE III
PARAMETERS OF THE TESTED DFIG

Rated power	1.0 kW	Rated voltage	110 V
Rated frequency	50 Hz	DC voltage	300 V
Stator/rotor turns ratio	0.33	R_s	1.01 Ω
R_r	0.88 Ω	L_m	90.1 mH
$L_{\sigma s}$	3.0 mH	$L_{\sigma r}$	3.0 mH

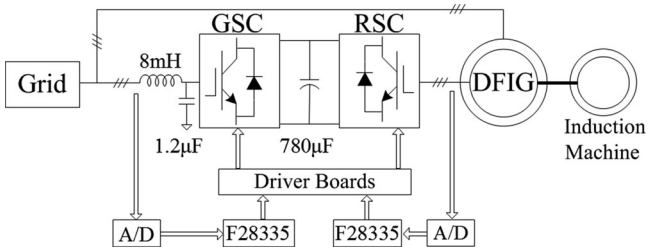

Fig. 13. Configuration of the experimental system.

When *Target I* is selected to implement the balanced total currents of DFIG system, according to (38) and Fig. 6(b), the transfer function of the negative-sequence voltage to the total current can be expressed as

$$F_{It}(s) = \frac{I_{td}}{U^+_{sd-}} = \frac{I_{tq}}{U^+_{sd-}} = \frac{G_{p2}(s) + (1 + G_{\mathrm{PI2}}(s)G_{p2}(s)) \cdot F_{Is}(s)}{1 + G_{\mathrm{PI2}}(s)G_{p2}(s) + G_{R2}(s)G_{p2}(s)}. \quad (39)$$

Fig. 8 shows the magnitude response of $F_{It}(s)$ with $R_g = 0.001\ \Omega$, $L_g = 0.25$ mH. It can be seen that the magnitude is reduced to -21.8 dB, whereas it rises to 0.7 dB with ROGI disabled. Thus, the high rejection capability on the negative-sequence voltage can be achieved, resulting in eliminating the negative-sequence components in the total currents.

From Fig. 6(b), it can be noted that, when *Target II* and *Target III* are adopted, the block diagram of the GSC are similar, while only the ROGI's feedbacks are different. Thus, the transfer function of the negative-sequence voltage to the active and reactive powers can be represented in a uniform expression and is given by

$$F_{\mathrm{PQ}}(s) = \frac{-P_t}{U^+_{sd-}} = \frac{Q_t}{U^+_{sd-}} = \frac{G_4(s)G_{p2}(s) + (1 + G_4(s)G_{\mathrm{PI2}}(s)G_{p2}(s)) \cdot F_{Is}(s)}{1 + G_{\mathrm{PI2}}(s)G_{p2}(s) + G_{R2}(s)G_4(s)G_{p2}(s)}. \quad (40)$$

Accordingly, the magnitude response of $F_{\mathrm{PQ}}(s)$ is presented in Fig. 9. Similar to Fig. 8, the magnitude response is reduced from 57.2 to -3.4 dB at $2\omega_1$ with the ROGI employed. Thus, the smooth total active or reactive power can be achieved using the proposed scheme.

Thus, it can be concluded that the proposed control strategy using ROGIs can ensure a satisfactory and acceptable rejection capability of the negative-sequence voltage disturbances on the twice pulsations of selected electromagnetic quantities, i.e., the generator torque, the total current, and the total active and reactive powers.

VI. SIMULATION RESULTS

In order to validate the effectiveness of the proposed collaborative control strategy, simulation model was developed based on MATLAB/Simulink, and the system schematic diagram is shown as Fig. 10. The parameters of the tested DFIG system is listed in Table I, where $k_{p1} = 5$, $k_{i1} = 30$, $k_{r1} = 10$ and $k_{p2} = 2$, $k_{i2} = 15$, $k_{r2} = 10$ are set in the RSC and GSC controllers, respectively. The switching frequencies for both the converters are 2.5 kHz. Since the mechanical time constant is much larger than the electromagnetic one, the rotor speed can be initially assumed at 1.2 p.u. in the following simulation tests. As required in [7], the wind turbine should withstand a 2% steady-state voltage unbalance and a 4% short-time voltage unbalance. In order to illustrate the available control capability of the proposed control strategy, a larger 10% steady-state and short-time unbalance is set in the simulations.

Fig. 11 shows the simulation results with 10% voltage unbalance, where the stator average active and reactive powers are set as 0.83 and 0.0 p.u., respectively. The RSC is controlled to suppress the torque ripples caused by the negative-sequence stator voltage, while the GSC is controlled with three different control targets. The control target was initially set to *Target I*, and then switched to *Target II* at 0.2 s and to *Target III* at 0.4 s, respectively. The proposed scheme using ROGIs was used for both the RSC and GSC in the simulation tests. As seen in Fig. 11(c), the generator torque is kept constant with this control scheme during network unbalance. Besides, three control targets for the GSC can be achieved, respectively. For a clear comparison, Table II summarizes the measured total current unbalance, the 100 Hz pulsations of the total active and reactive powers and the dc-link voltage. When *Target I* is adopted, only 0.7% total current unbalance can be found, and the total active and reactive power pulsations can be suppressed to $\pm 9.3\%$ and $\pm 7.5\%$. When *Target II* is selected at 0.2 s, the total active power pulsation decreases to $\pm 0.5\%$. Besides, the dc-link voltage fluctuation is reduced to $\pm 1.3\%$. However, the total reactive power pulsations will increase to $\pm 16.2\%$. Similarly, when *Target III* was selected, the total reactive power pulsation is suppressed to $\pm 1.1\%$, but the active power pulsations become $\pm 16.2\%$.

Further tests with different control schemes were implemented to show the advantage of the proposed control scheme. As indicated in [29], since the PI-R controller has a wider bandwidth around the fundamental frequency (50 Hz) than the P-R controller, a better and faster power tracking capability can be achieved by PI-R controller. Thus, in this paper, the PI-R controller is adopted in the simulation tests. The simulation results of these two different control strategies, i.e., the PI-R method and the proposed method, are provided in Fig. 12 during a 10% short-time voltage unbalance from 0.1 to 0.4 s. The stator active and reactive powers are also set at 0.83 and 0 p.u., respectively, the same as Fig. 11. In this test, the RSC is controlled to reduce the torque ripples while the GSC is controlled to remove the total active power pulsations, i.e., *Target II*. Fig. 12(a) shows the simulation results using the PI + R control scheme. Since the decompositions of the positive- and negative-sequence components are still involved in the calculations of the negative-sequence current references, the dynamic

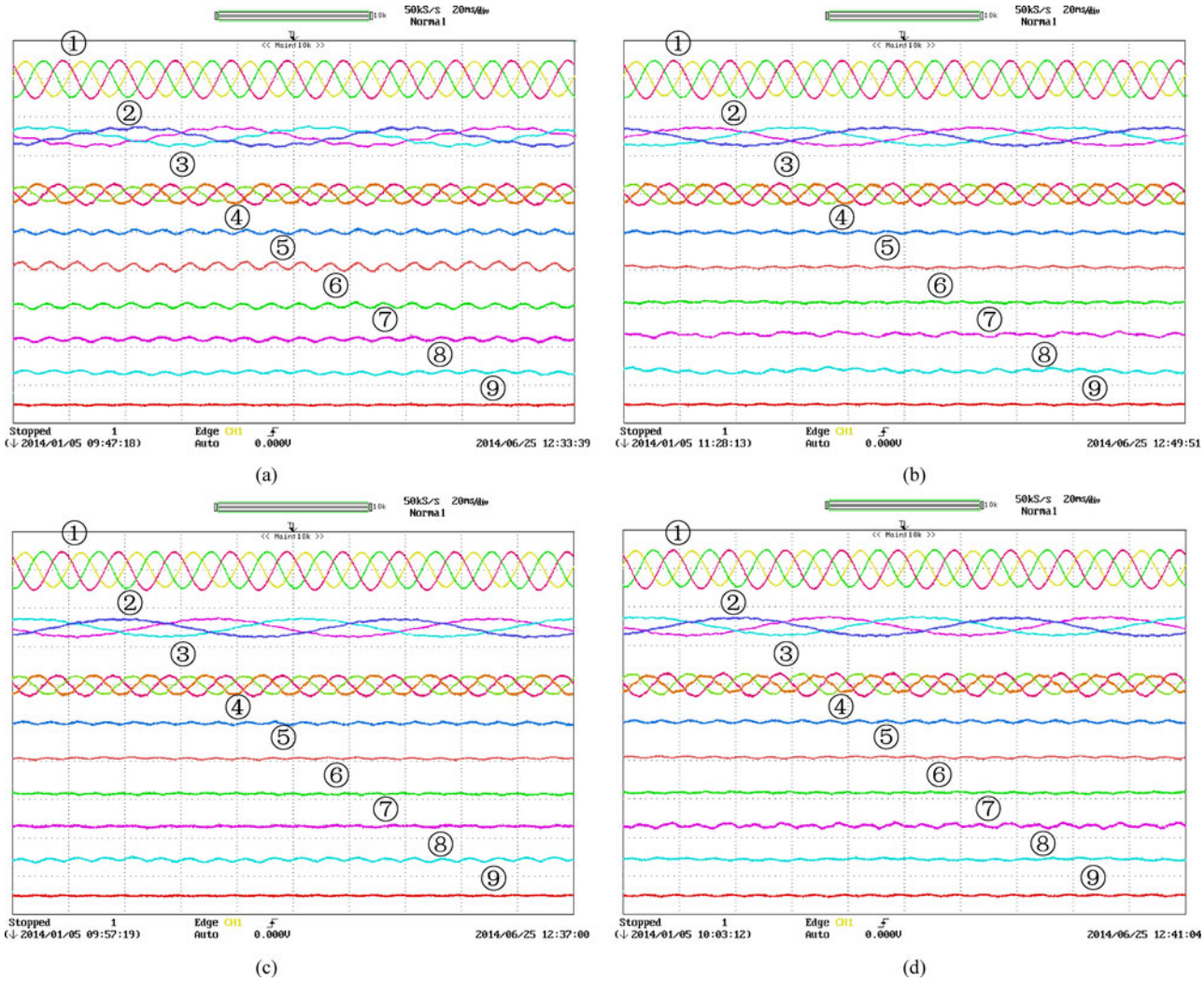

Fig. 14. Measured waveforms of the system steady responses (20 ms/div) [① U_{sabc} stator line voltage (300 V/div), ② I_{rabc} rotor current (10 A/div), ③ I_{tabc} total current (30 A/div), ④ P_s stator active power (1500 W/div), ⑤ Q_s stator reactive power (1500 Var/div), ⑥ T_e generator torque (20 N·m/div), ⑦ P_t total active power (1500 W/div), ⑧ Q_t total reactive power (1500 Var/div), ⑨ $V_{\rm dc}$ dc-link voltage (60 V/div)]. (a) PI control under the unbalanced grid voltage conditions. (b) PI control with ROGIs for *Target I*. (c) PI control with ROGIs for *Target II*. (d) PI control with ROGIs for *Target III*.

responses would be deteriorated with a longer transient process. As shown in Fig. 12(B) (d) and (e), the generator torque and the total active power has a relatively smooth transient process than those in Fig. 12(A). This is mainly because the generator torque and the total active power are directly controlled in the proposed control scheme. Besides, the calculations of the negative-sequence current references are eliminated, which can assist the DFIG smoothly back to the normal operation. It can be also seen that the collaborate control of both the RSC and GSC can improve the overall DFIG system performance under unbalanced grid voltage conditions, by reducing the torque ripples and removing the total active power pulsations. Besides, the dc-link voltage fluctuations are also suppressed.

VII. Experimental Validations

Experimental tests were carried out on a laboratory setup of 1.0 kW DFIG system with the parameters and configurations as shown in Table III and Fig. 13, respectively. In this setup, the generator is driven by an induction motor and a Chroma programmable ac source 61704 was used to simulate the unbalanced supply. Both DFIG's RSC and GSC are controlled separately by two TI TMS320F28335 DSPs with a sampling frequency of 10 kHz. The SVM technique is used to generate the switching pulse with a switching frequency of 10 kHz.

TABLE IV
Comparisons Among the Alternative Control Targets During Network Unbalance

Control targets	No ROGI	Target I	Target II	Target III
I_t unbalance (%)	8.2	**1.3**	6.5	5.9
P_t pulsation (%)	±8.3	±4.3	±**1.1**	±8.1
Q_t pulsation (%)	±10.4	±4.8	±7.2	±**1.2**
T_e pulsation (%)	±9.6		±**1.0**	

In the following tests, the average stator active and reactive powers are set as $P_{s0} = 1000$ W (export of active power from the generator to the network), $Q_{s0} = 0$ Var, respectively. The DFIG speed was initially fixed at 800 r/min (0.8 p.u., equivalent to 40 Hz), where the synchronous speed is 1000 r/min. The

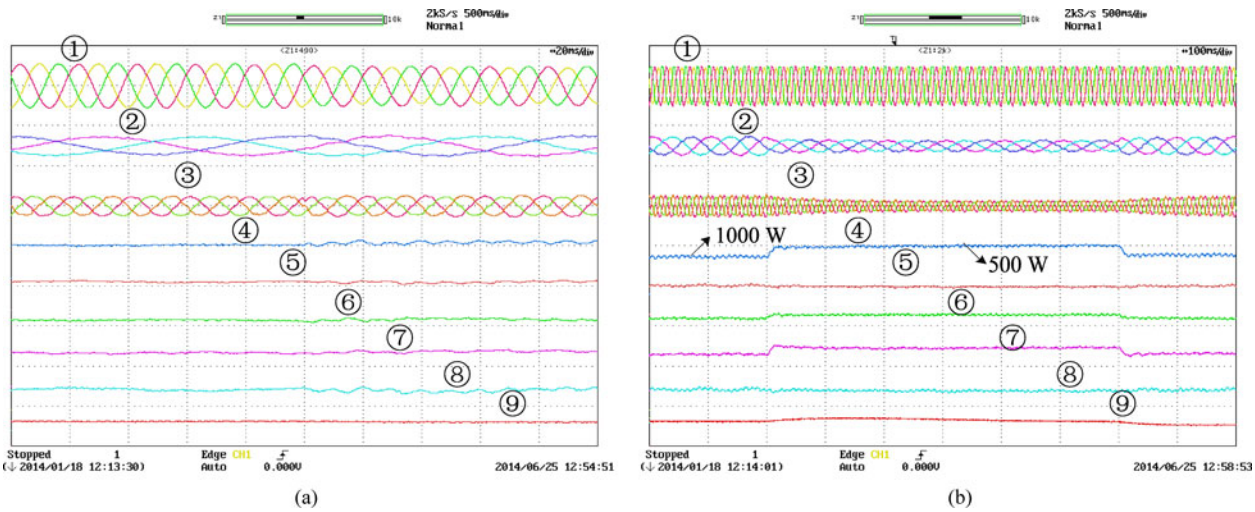

Fig. 15. Measured waveforms of the system transient responses [① U_{sabc} stator line voltage (300 V/div), ② I_{rabc} rotor current (10 A/div), ③ I_{tabc} total current (30 A/div), ④ P_s stator active power (1500 W/div), ⑤ Q_s stator reactive power (1500 Var/div), ⑥ T_e generator torque (20 N·m/div), ⑦ P_t total active power (1500 W/div), ⑧ Q_t total reactive power (1500 Var/div), ⑨ $V_{\rm dc}$ dc-link voltage (60 V/div)]. (a) Transient voltage unbalance (20 ms/div). (b) Active power up- and down-steps (100 ms/div).

voltage imbalance is around 5.4% and the preexisting fifth and seventh harmonic components are 0.97% and 0.52%, respectively. Besides, all the waveforms are acquired by a YOKOGAWA DL750 scope recorder.

A. Steady Responses

Fig. 14 shows the steady-state performance of DFIG on the proposed control. In Fig. 14(a), the conventional PI controllers are used for the RSC and GSC. The rotor current contains 90 Hz (50 + 40 Hz) due to the opposite direction of the negative-sequence rotor current. Considering that the fundamental frequency in rotor winding is 10 Hz (50 − 40 Hz), this negative-sequence component can be regarded as ninth-order harmonic component which is about 4.5%. The stator active and reactive powers contain significant 100 Hz oscillations, which are around ±9.1% and ±12.5%. Most importantly, the torque ripples increase to ±9.6%, which may pose the great stress on the drive train. Fig. 14(b)–(d) shows the experimental results of the three control targets with the proposed control scheme. Since the control target for the RSC is selected to suppress the torque ripples, the torque ripples can be suppressed to ±1.0%. When *Target I* for the GSC is adopted, the imbalance of total currents was reduced from 8.2% to 1.3%. By selecting *Target II*, the total active power oscillations decreased to ±1.1%, while the total reactive power oscillations increased to ±7.2%. For *Target III*, the total reactive power oscillation was ±1.2%, and the total active power oscillations rise to ±8.1%. Since the larger dc capacitor provides the adequate buffer for the energy transmission, the dc voltage fluctuations are not apparent here.

The total current unbalance, the 100 Hz pulsations of the generator torque ripples, the total active and reactive powers in Fig. 14 are listed and compared in Table IV, where three control targets were adopted. It is evident that the results demonstrate the availability of the proposed control strategy in reducing torque ripples, or depressing the outputted current unbalance, or smoothing the total generated powers.

B. Transient Response

Further tests were carried out to discuss the system dynamic responses with the proposed control strategy. According to the operation of practical DFIG systems and network requirements, the torque and the total active power outputted into the grid are the main attentions. Thus, *Target II* is selected for the GSC control objective and the RSC is controlled to reduce the torque ripples in this test.

Fig. 15 shows the dynamic responses where the operation condition is the same as that in Fig. 14. The dynamic responses of the DFIG system at the moment of the negative-sequence voltage appearing are shown in Fig. 15(a). When the grid voltage unbalance occurs, the torque ripples and total active power pulsations can still be controlled within ±1.1% and ±1.0%, respectively. Besides, step changes of the output active power from 1000 to 500 W, and then back to 1000 W are exhibited in Fig. 15(b). As seen, the proposed control strategy can still ensure the constant generator torque and constant power from the overall system during network unbalance.

From Figs. 14 and 15, it is noted that the proposed collaborate control strategy with ROGIs can effectively mitigate the negative impacts caused by the voltage disturbances for the overall DFIG system so as to meet the grid requirements. Besides, it is capable of providing both acceptable steady-state performance and satisfactory dynamic responses for the overall DFIG system during network unbalance.

VIII. Conclusion

This paper proposes a collaborative control for DFIG's RSC and GSC under unbalanced grid voltage conditions. The RSC

is controlled to reduce torque ripples, while either the current unbalance, or the oscillations in the total active or reactive power is suppressed as the different control targets for the GSC. The ROGIs in the positive synchronous reference frame were employed to restrain the pulsating components. Furthermore, the proposed control scheme using ROGIs can provide: 1) simple implementation without the calculations of the negative-sequence current reference; and 2) fast dynamic responses due to the avoidance of the sequential decompositions. Finally, simulation and experimental results during network unbalance are given to validate the feasibility and availability of the proposed collaborate control scheme.

REFERENCES

[1] F. Blaabjerg, M. Liserre, and K. Ma, "Power electronics converters for wind turbine systems," *IEEE Trans. Ind. Appl.*, vol. 48, no. 2, pp. 708–719, Mar./Apr. 2012.

[2] Z. Chen, J. M. Guerrero, and F. Blaabjerg, "A review of the state of the art of power electronics for wind turbines," *IEEE Trans. Power Electron*., vol. 24, no. 8, pp. 1859–1875, Aug. 2009.

[3] J. M. Carrasco, L. G. Franquelo, J. T. Bialasiewicz, E. Galvan, R. C. P. Guisado, A. M. Prats, J. I. Leon, and N. Moreno-Alfonso, "Power-electronic systems for the grid integration of renewable energy sources: A survey," *IEEE Trans. Ind. Electron.*, vol. 53, no. 4, pp. 1002–1016, Aug. 2006.

[4] *Grid Code—High and Extra High Voltage*, E.ON Netz GmbH, Bayreuth, Germany, 2006.

[5] *Requisitos de respuesta frente a huecos de tension de las instalaciones de produccion de regimen especial, PO12.3*, REE, Madrid, Spain, 2005.

[6] *Grid Connection of Wind Turbines to Networks with Voltages below 100 kV*, Energinet, Fredericia, Denmark, 2004.

[7] *Technical Rule for Connecting Wind Farm to Power System*, GB/T 19963-2011, 2012.

[8] F. K. A. Lima, A. Luna, S. Member, P. Rodriguez, E. H. Watanabe, S. Member, and F. Blaabjerg, "Rotor voltage dynamics in the doubly fed induction generator during grid faults," *IEEE Trans. Power Electron.*, vol. 25, no. 1, pp. 118–130, Jan. 2010.

[9] S. Xiao, G. Yang, H. L. Zhou, and H. Geng, "An LVRT control strategy based on flux linkage tracking for DFIG-based WECS," *IEEE Trans. Ind. Electron.*, vol. 60, no. 7, pp. 2820–2832, Jul. 2013.

[10] L. Xu and Y. Wang, "Dynamic modeling and control of DFIG-based wind turbines under unbalanced network conditions," *IEEE Trans. Power Syst.*, vol. 22, no. 1, pp. 314–323, Feb. 2007.

[11] Y. Zhou, P. Bauer, J. A. Ferreira, and J. Pierik, "Operation of grid-connected DFIG under unbalanced grid voltage condition," *IEEE Trans. Energy Convers.*, vol. 24, no. 1, pp. 240–246, Mar. 2009.

[12] M. I. Martinez, G. Tapia, A. Susperregui, and H. Camblong, "DFIG power generation capability and feasibility regions under unbalanced grid voltage conditions," *IEEE Trans. Energy Convers.*, vol. 26, no. 4, pp. 1051–1062, Dec. 2011.

[13] J. B. Hu, Y. K. He, L. Xu, and B. W. Williams, "Improved control of DFIG systems during network unbalance using PI-R current regulators," *IEEE Trans. Ind. Electron.*, vol. 56, no. 2, pp. 439–451, Feb. 2009.

[14] P. Van-Tung and H.-H. Lee, "Performance enhancement of stand-alone DFIG systems with control of rotor and load side converters using resonant controllers," *IEEE Trans. Ind. Appl.*, vol. 48, no. 1, pp. 199–210, Jan./Feb. 2012.

[15] T. K. A. Brekken and N. Mohan, "A novel doubly-fed induction wind generator control scheme for reactive power control and torque pulsation compensation under unbalanced grid voltage conditions," in *Proc. Power Electron. Spec. Conf.*, vol. 2, 2003, pp. 760–764.

[16] T. K. A. Brekken and N. Mohan, "Control of a doubly fed induction wind generator under unbalanced grid voltage conditions," *IEEE Trans Energy Convers.*, vol. 22, no. 1, pp. 129–135, Mar. 2007.

[17] M. Reyes, P. Rodriguez, S. Vazquez, A. Luna, R. Teodorescu, and J. M. Carrasco, "Enhanced decoupled double synchronous reference frame current controller for unbalanced grid-voltage conditions," *IEEE Trans. Power Electron.*, vol. 27, no. 9, pp. 3934–3943, Sep. 2012.

[18] I. Etxeberria-Otadui, U. Viscarret, M. Caballero, A. Rufer, and S. Bacha, "New optimized PWM VSC control structures and strategies under unbalanced voltage transients," *IEEE Trans. Ind. Electron.*, vol. 54, no. 5, pp. 2902–2914, Oct. 2007.

[19] G. Q. Shen, X. C. Zhu, J. Zhang, and D. H. Xu, "A new feedback method for PR current control of LCL-filter-based grid-connected inverter," *IEEE Trans. Ind. Electron.*, vol. 57, no. 6, pp. 2033–2041, Jun. 2010.

[20] H. Geng, C. Liu, and G. Yang, "LVRT capability of DFIG-based WECS under asymmetrical grid fault condition," *IEEE Trans. Ind. Electron.*, vol. 60, no. 6, pp. 2495–2509, Jun. 2013.

[21] L. Xu, "Coordinated control of DFIG's rotor and grid side converters during network unbalance," *IEEE Trans. Power Electron.*, vol. 23, no. 3, pp. 1041–1049, May 2008.

[22] J. B. Hu, H. L. Xu, and Y. K. He, "Coordinated control of DFIG's RSC and GSC under generalized unbalanced and distorted grid voltage conditions," *IEEE Trans. Ind. Electron.*, vol. 60, no. 7, pp. 2808–2819, Jul. 2013.

[23] J. B. Hu and Y. K. He, "Reinforced control and operation of DFIG-based wind-power-generation system under unbalanced grid voltage conditions," *IEEE Trans. Energy Convers.*, vol. 24, no. 4, pp. 905–915, Dec. 2009.

[24] C. J. Liu, F. Blaabjerg, W. J. Chen, and D. H. Xu, "Stator current harmonic control with resonant controller for doubly fed induction generator," *IEEE Trans. Power Electron.*, vol. 27, no. 7, pp. 3207–3220, Jul. 2012.

[25] C. A. Busada, S. G. Jorge, A. E. Leon, and J. A. Solsona, "Current controller based on reduced order generalized integrators for distributed generation systems," *IEEE Trans. Ind. Electron.*, vol. 59, no. 7, pp. 2898–2909, Jul. 2012.

[26] P. Zhou, Y. K. He, and D. Sun, "Improved direct power control of a DFIG-based wind turbine during network unbalance," *IEEE Trans. Power Electron.*, vol. 24, no. 11, pp. 2465–2474, Nov. 2009.

[27] J. Hu and Y. He, "DFIG wind generation systems operating with limited converter rating considered under unbalanced network conditions—Analysis and control design," *Renew. Energy*, vol. 36, no. 2, pp. 829–847, 2011.

[28] H. Nian, Y. P. Song, P. Zhou, and Y. K. He, "Improved direct power control of a wind turbine driven doubly fed induction generator during transient grid voltage unbalance," *IEEE Trans. Energy Convers.*, vol. 26, no. 3, pp. 976–986, Sep. 2011.

[29] C. Lascu, L. Asiminoaei, I. Boldea, and F. Blaabjerg, "Frequency response analysis of current controllers for selective harmonic compensation in active power filters," *IEEE Trans. Ind. Electron.*, vol. 56, no. 2, pp. 337–347, Feb. 2009.

Peng Cheng was born in Chaoyang, China. He received the B.Sc. degree in electrical engineering from the College of Electrical Engineering, Zhejiang University, Hangzhou, China, in July 2011, where he is currently working toward the Ph.D. degree.

His current research interests include motor control with power electronics devices in renewable-energy conversion, particularly the control and operation of doubly fed induction generators for wind power generation.

Heng Nian (M'09) received the B.Eng. and M.Eng. degrees from the HeFei University of Technology, Hefei, China, and the Ph.D. degree from Zhejiang University, Hangzhou, China, in 1999, 2002, and 2005, respectively, all in electrical engineering.

From 2005 to 2007, he was a Postdoctoral Researcher with the College of Electrical Engineering, Zhejiang University, where he has been an Associate Professor since 2007. His current research interests include the optimal design and operation control for wind power generation system.